conserved. This is not surprising since quarks can emit or absorb gluons, which carry color. Only if we add the color charge of the gluon field, represented by the second term on the right-hand side of Eq. (13.84), is a conserved color current obtained.

In view of the similarity in form of $\mathcal{L}_{\mathrm{QCD}}$ to $\mathcal{L}_{\mathrm{QED}}$, many of the well-known other formal properties carry over. We refrain from systematically developing this here, even though we will call upon these similarities as needed in further developments.

14 Perturbative QCD

14.1 Feynman rules

The nonabelian gauge theory of quarks and gluons, proposed in section 13.5 and called QCD, has widely been accepted as the fundamental theory of strong interactions, with both quarks and gluons being the carriers of the strong-interaction charge [123]. The evidence for the validity of QCD as a dynamic theory governing hadronic reactions is overwhelming, and this is not the place where this matter should be argued. Rather, we will show how QGP-related practical results can be derived from the complex theoretical framework. There are many books dealing with more applications of QCD and the interested reader should consult these for further developments [110, 194, 280].

Akin to QED, QCD is a 'good' renormalizable theory. QCD is known to be also an *asymptotically free* theory, viz., the running coupling constant α_{s}, see Eq. (14.12), is a diminishing function as the energy scale increases. Therefore, the high-energy, or, equivalently, the short-distance behavior is amenable to a perturbative expansion. On the other hand, perturbative QCD has 'fatal' defects at large distances, which are signaled by the growth and the ultimate divergence of α_{s} as the scale of energy diminishes (infrared 'slavery'). Consequently, at any reasonable physical distance of relevance to the 'macroscopic' QGP, we have to deal with an intrinsically strongly coupled, nonperturbative physical system. A perturbative treatment ignores this, and, in principle, must be unreliable in problems in which the confinement scale becomes relevant. The question of when exactly this occurs will be one of the important issues we will aim to resolve, using as criterion $\alpha_{\mathrm{s}} \leq 1$.

The perturbative approach, which applies to short-distance phenomena, has been tested extensively in high-energy processes. When the 'short distance' grows and approaches 0.5 fm, the perturbative expansion of QCD may still apply insofar as its results are restricted to the physics occurring in the deconfined, viz., QGP, phase. The rules of perturbative QCD follow the well-known Feynman rules of QED, allowing for the glue–glue

interactions. However, unlike QED, in which the expansion parameter is $\alpha/\pi = \mathcal{O}(10^{-3})$, we must deal in case of QCD with 'strong' coupling, which is nearly 30–100 times greater than that in QED. Therefore, even when a perturbative description is suitable, some effort to reach the required precision is often necessary, involving the inclusion of higher-order Feynman diagrams.

The quadratic terms 'ψ^2' and 'A^2' in the Lagrangian $\mathcal{L}_{\text{QCD}}$ define free quark and gluon fields which are described by propagators of the same form as those for electrons and photons in QED. The terms of third and fourth order in $\mathcal{L}_{\text{QCD}}$ give rise to interaction vertices among the free propagators of quarks and gluons. There is a quark–gluon vertex, and three-gluon and four-gluon vertices. Propagators and vertices can be combined to generate Feynman diagrams in all possible ways.

One technical difference arises between QED and QCD, which is associated with the difficulties of gauge theories with regard to gauge fixing. To ensure gauge invariance of QCD, it is convenient to introduce into the perturbative expansion fictitious (virtual) particles called Fadeev–Popov (FP) ghosts, which never appear in physical states, but are to be included in all virtual processes. FP fields carry color, and satisfy Fermi statistics even though they propagate like spin-zero particles – hence the name 'ghost'. The complete Lagrangian in a Lorentz-covariant gauge reads

$$\mathcal{L}_{\text{QCD}} = -\frac{1}{4}(F_a^{\mu\nu} F_{\mu\nu}^a)^2 + \xi(\partial_\mu A_\mu^a)^2 + \bar{\phi}(\partial^\mu \delta_{ab} + g f^{asb} A_\mu^s)\partial^\mu \phi^b$$
$$+ \sum_{\text{f}} \overline{\Psi}_{\text{f}}\big[\gamma^\mu(\partial_\mu + g A_\mu^s) - m_{\text{f}}\big]\Psi_{\text{f}}, \tag{14.1}$$

where the summation over color indices is implied and the second term in Eq. (14.1) is the gauge-fixing term and the third term formed with the scalar fields ϕ introduces the Fadeev–Popov ghosts. We note that it is possible to work in a non-Lorentz-covariant gauge and to obtain results without introducing ghosts, instead using longitudinal and transverse gluons as identifiable degrees of freedom, with longitudinal gluons not present in any asymptotic physical states. For further discussion, we refer to relevant textbooks [110, 194, 280].

We skip the technical details regarding the development of the perturbative QCD, and only collect for the convenience of the reader and further reference the building blocks of the perturbative expansion required for evaluation of Feynman diagrams, i.e., propagators and vertices of QCD, presented in a self-explanatory notation. Latin indices refer to color degrees of freedom, Greek indices to space, q to quarks, g to gluons, and FP to the ghost field.

We have
the quark propagator,

$$(S_{\alpha\beta}(p))^{ab} = \left(\frac{\delta_{ab}}{\gamma p - m + i\varepsilon}\right)_{\alpha\beta}, \tag{14.2}$$
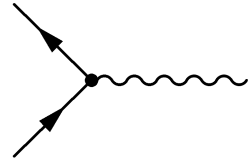
the gluon propagator,

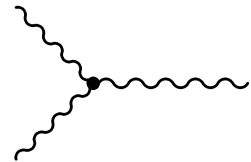$$i(D_{\mu\nu}(k))^{ab} = \frac{\delta_{ab}g_{\mu\nu}}{k^2 + i\varepsilon}, \tag{14.3}$$

the quark–antiquark–gluon vertex,

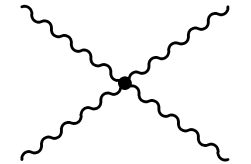$$(\Gamma^{\mu,c}_{\mathrm{qqg}})^{ab}_{\alpha\beta} = g(t^c)^{ab}(\gamma^\mu)_{\alpha\beta}, \tag{14.4}$$

the three-gluon vertex,

$$(\Gamma^{\mu\nu\sigma}_{\mathrm{g}^3})_{abc} = gf_{abc}[g^{\mu\nu}(k-p)^\sigma + \text{cyclic permutations}], \tag{14.5}$$

the four-gluon vertex,

$$(\Gamma^{\mu\sigma\nu\tau}_{\mathrm{g}^4})_{abcd} = g^2 f_{iab}f_{icd}[(g^{\mu\sigma}g^{\nu\tau} - g^{\mu\tau}g^{\nu\sigma}) + \text{cyclic permutations}], \tag{14.6}$$
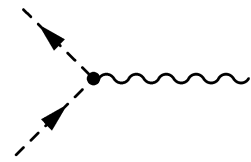
the ghost propagator,

$$(G_{\mathrm{FP}}(k))^{ab} = \frac{\delta_{ab}}{k^2 + i\varepsilon}, \tag{14.7}$$

and the gluon–ghost–ghost vertex,

$$(\Gamma^\mu_{\mathrm{gFP}})_{abc} = -gf_{abc}p^\mu. \tag{14.8}$$

For any given process, for which a Feynman diagram is drawn using the lines and vertices as illustrated above, the above list allows one to compose the mathematical expression for the amplitude of the process. Very few additional rules need to be remembered, such as integration over the 'spare' momentum variables in the diagram, an overall coefficient (-1) for each fermion and ghost loop, and the absence of ghost propagators that do not begin and end in a vertex.

While the forms of the above-stated propagators and vertices change in a finite-temperature environment, which is mainly being addressed in this book, the structure of the perturbative expansion generated by these quantities remains the same. The construction of a matrix element and cross section requires wave-function-normalization factors, and flux factors that are all quite standard in this context, and available in numerous introductory textbooks. In these aspects, there is no difference between QCD and any other theoretical framework, such as QED. However, we recall that, in order to obtain a cross section, we average over initial states, and sum over final states, which now will include, in particular, the color degree of freedom.

14.2 The running coupling constant

The free-gluon propagator, which, like in QED, is proportional to $1/q^2$, implies that the 'free' color force falls off like $1/r$. The gluon propagator is, even in the perturbative vacuum, modified by scattering from virtual quark–gluon fluctuations. This 'dressing' of the propagator leads to the running, q^2-dependent coupling constant, and the dressed physical gluon propagator is expected to significantly differ from the free one. In order to see how this comes about, we consider the loop diagrams corresponding to the virtual and momentary creation of a pair of colored particles in the vacuum. For the contribution of fermions to the polarization loop, this process is very similar to the case of QED.

There are two more elementary processes that contribute to the covariant form of perturbative QCD, namely the gluon loop and the ghost loop, The vacuum-polarization loop $\Pi(q^2)$ comprises these three terms:

It is customary to sum the chain of higher-order diagrams, containing series of all different loops,

$$D(q^2) \;=\; D_0 \;+\; D_0\Pi D_0 \;+\; D_0\Pi D_0\Pi D_0 \;+\cdots$$

$$D(q^2) = \frac{D_0(q^2)}{1 - \Pi(q^2)D_0(q^2)}, \tag{14.9}$$

such that the gluon is dressed by the consecutive interactions with the vacuum polarization. The effect of the quark, glue, and ghost loops combines in the coefficient b_0, Eq. (14.14), of the vacuum-polarization function. Introducing a high momentum (ultraviolet) cutoff to secure the convergence, for massless quarks and gluons, $\Pi(q^2)$ takes the form

$$\Pi(q^2) = \frac{g^2 b_0}{8\pi}(-q^2)\ln\left(\frac{-q^2}{\mu^2}\right), \tag{14.10}$$

where μ is a reference momentum absorbing the cutoff, and defined by the renormalization condition: $\Pi(q^2 = -\mu^2) = 0$.

The value of μ^2 introduces, in general, a dependence on renormalization. In this order, this dependence can be absorbed into the choice of the value of the coupling constant at a given transfer of momentum; see Eq. (14.13) below. The overall sign of Π, Eq. (14.10), is related to the sign of b_0, and is opposite to that of the polarization function of fermions alone (QED) as long as the flavor number $n_{\rm f} < (11/2)n_{\rm c}$. The sign of the polarization function is quite important, as we shall see.

With the help of Eq. (14.10), we obtain

$$g^2 i D(q^2) = \frac{1}{q^2} \frac{g^2}{1 + \dfrac{g^2 b_0}{8\pi}\ln\left(\dfrac{-q^2}{\mu^2}\right)}. \tag{14.11}$$

The last factor acts as a momentum-dependent modification of the strong coupling constant g^2. It is therefore convenient to introduce the 'running' coupling constant $\alpha_{\rm s}(q^2)$,

$$\boxed{\alpha_{\rm s}(q^2) = \frac{2}{b_0 \ln(-q^2/\Lambda^2)},} \tag{14.12}$$

with

$$\Lambda^2 = \mu^2 \exp\left(-\frac{8\pi}{b_0 g^2}\right), \quad \alpha_{\rm s} = \frac{g^2}{4\pi}. \tag{14.13}$$

The above expression applies for positive b_0, and, in this case, we see that, for an increasing q^2, the physical coupling constant $\alpha_{\rm s}(q^2)$ decreases; QCD is asymptotically free.

In the case of QED, the sign of b_0 is opposite, and the effective coupling constant is finite at large distances, i.e., at small q^2, and increases with q^2. The reference scale μ^2 in Eq. (14.11) can be chosen to be at zero momentum (infinite distance) and this corresponds to the usual definition

of the electron charge. This choice is not possible in case of QCD, since the interaction strength becomes infinite for $\mu^2 \to 0$.

Λ is the dimensional parameter which emerges in perturbative QCD. The original dimensionless coupling constant g^2 has been absorbed in the scale Λ governing the change of the running coupling constant $\alpha_{\rm s}$, in the process of transition from Eq. (14.11) to Eq. (14.12). This so-called 'transmutation' of the dimensionless scale of strength into a dimensioned strength parameter of the interaction also absorbs the scale dependence introduced by the choice of μ^2.

In the limit that all quark masses vanish, $m_i \to 0$, Λ is the only dimensional parameter of the theory of strong interactions. It is believed that the world of hadrons (except the pion) is not decisively dependent on the scale of the quark mass. Thus, it seems that Λ alone controls the mass and the size of the massive hadrons (nucleons and heavy non-strange mesons). To understand this, we would need to express the vacuum structure in terms of Λ, a problem which has not been resolved.

The *measurable* dimensioned parameter Λ^2 determines the strength of the interaction at a given momentum scale. This approach applies quite accurately for energy–momentum scales above the mass of the b quark, as we shall see later in Fig. 14.1, where the value of $\Lambda \simeq 90\pm15$ MeV applies. At small q^2, i.e., at 'large' distances, the coupling constant Eq. (14.12) diverges within the perturbative approach. The magnitude of the strong charge must be defined at some finite momentum scale, which has in recent years, been chosen to be the mass of the Z^0 boson, $\mu \equiv M_{\rm Z^0} \simeq 91.19$ GeV.

Since we have more than one quark, the important coefficient b_0 is composed of a term proportional to the number of 'active' flavors $n_{\rm f}$, i.e., those with $|q^2| > 4m_{\rm f}^2$. The number of colors $n_{\rm c} = 3$ enters the glue loop: in the gluon loop diagram, each external leg requires the triple-glue vertex, Eq. (14.5), which invokes relation Eq. (13.63) or equivalently Eq. (13.60) for two external gluon legs. b_0 for $SU_{\rm c}(3)$ assumes the form

$$b_0 = \frac{1}{2\pi}\left(\frac{11}{3}n_{\rm c} - \frac{2}{3}n_{\rm f}\right). \tag{14.14}$$

The spin s of particles contributing to the vacuum polarization is found to be the key ingredient controlling the sign of b_0 [149],

$$b_0^{\rm s} = \frac{(-)^{2s}}{2\pi}\left((2s)^2 - \frac{1}{3}\right), \tag{14.15}$$

which leads to Eq. (14.14), introducing $s = 1$ for gluons and $s = \frac{1}{2}$ for quarks. Equation (14.15) shows why for $s = 0, \frac{1}{2}$ the same (negative) sign appears, whereas for gluons with $s = 1$ there is a change of sign. Photons do not interact with photons and hence this issue did not arise in QED.

14.3 The renormalization group

The question of what happens as we carry out the same procedures in higher orders in perturbation theory now arises. A considerable amount of effort went into designing a scheme for computing the observable effects in QED, and this experience has been generalized to the more complex case of QCD. We will restrict ourselves to a few elements of the *renormalization-group* approach relevant to our presentation, sidestepping many interesting and intricate questions, which are addressed in, e.g., [110, 194, 280].

The renormalization-group approach allows us to understand the variation of the physical observables in terms of the momentum dependence of the coupling constant α_s. A functional dependence is found demanding that the result of a physical measurement (say a cross section σ) be invariant with respect to the process of renormalization, and, in particular, the observable (cross section) can not depend explicitly on the choice of the '(re)normalization' point μ^2,

$$\mu \frac{d}{d\mu} \sigma(p_i; \alpha_s, m; \mu) = 0. \tag{14.16}$$

Accounting for both a direct and an indirect dependence on μ in Eq. (14.16),

$$\left(\mu \frac{\partial}{\partial \mu} + \mu \frac{\partial \alpha_s}{\partial \mu} \frac{\partial}{\partial \alpha_s} + \mu \frac{\partial m}{\partial \mu} \frac{\partial}{\partial m} + \cdots \right) \sigma = 0. \tag{14.17}$$

It is convenient to define

$$\boxed{\mu \frac{\partial \alpha}{\partial \mu} \equiv \beta(\alpha_s)} \tag{14.18}$$

and

$$\boxed{-\frac{\mu}{m} \frac{\partial m}{\partial \mu} \equiv \gamma(\alpha_s),} \tag{14.19}$$

and thus:

$$\left(\mu \frac{\partial}{\partial \mu} + \beta(\alpha_s) \frac{\partial}{\partial \alpha_s} - \gamma(\alpha) m \frac{\partial}{\partial m} + \cdots \right) \sigma = 0. \tag{14.20}$$

Equation (14.20) allows us to understand the behavior of the observable σ, and it establishes the behavior of σ under simultaneous changes of reference scale μ, coupling constant, and mass.

Equations (14.18) and (14.19) establish how the parameters of QCD vary once they are known at some given scale. Therefore, precise knowledge of the renormalization functions β and γ is, to a large degree, equiv-

alent to finding a practical 'solution' of QCD. For this reason, these quantities have attracted a lot of attention. We will look at the perturbative results only, in terms of a power expansion in α_s [255]:

$$\beta^{\text{pert}} = -\alpha_s^2 \big[\, b_0 + b_1\alpha_s + b_2\alpha_s^2 + \cdots \,\big], \qquad (14.21)$$

$$\gamma_m^{\text{pert}} = \alpha_s \big[\, w_0 + w_1\alpha_s + w_2\alpha_s^2 + \cdots \,\big]. \qquad (14.22)$$

For the $SU(3)$ gauge theory with n_f fermions only, the first two terms (two 'loop' orders) are renormalization-scheme-independent. When a dependence on the renormalization scheme arises, this means that compensating terms, which remove scheme dependence, are obtained on evaluating in the same scheme the physical process considered. For what follows in this book, this so-called two-loop level of perturbative expansion for β^{pert} and γ_m^{pert} is sufficient.

We have

$$b_0 = \frac{1}{2\pi}\left(11 - \frac{2}{3}n_f\right), \qquad b_1 = \frac{1}{4\pi^2}\left(51 - \frac{19}{3}n_f\right), \qquad (14.23)$$

$$w_0 = \frac{2}{\pi}, \qquad\qquad\qquad w_1 = \frac{1}{12\pi^2}\left(101 - \frac{10}{3}n_f\right). \qquad (14.24)$$

The number n_f of 'active' fermions depends on the scale μ. Assuming that the two lightest quarks are effectively massless,

$$n_f(\mu) = 2 + \sum_{i=\text{s,c,b,t}} \sqrt{1 - \frac{4m_i^2}{\mu^2}\left(1 + \frac{2m_i^2}{\mu}\right)}\,\Theta(\mu - 2m_i), \qquad (14.25)$$

with values of m_i evaluated, in principle, for the energy scale being considered. There is a very minimal impact of the values of quark-mass thresholds in Eq. (14.25), on the running behaviors of the coupling constant and quark masses.

14.4 Running parameters of QCD

For the purpose of QGP studies, we are interested in understanding how the strength of the QCD interaction and the quark mass change with the energy scale. The simplest way to obtain this result is to integrate the first-order differential equation, Eqs. (14.18) and (14.19), given initial values of $\alpha_s(M)$ and $m_i(M)$, using the perturbative definition of the functions β and γ, Eqs. (14.21) and (14.22), in terms of the perturbative expansion Eqs. (14.23) and (14.24).

For the determination of the coupling constant, it has become common to refer to the value of $\alpha_s(M_Z = 91.19\,\text{GeV})$. We use, in Fig. 14.1, the value [136] $\alpha_s(M_Z) = 0.1182 \pm 0.002$ (thick solid lines). The thin solid
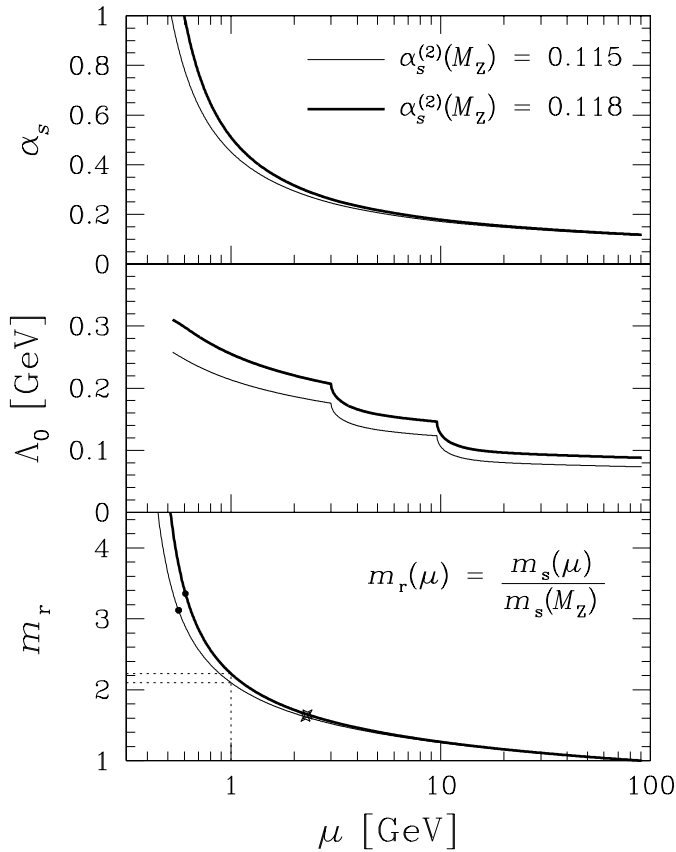
Fig. 14.1. $\alpha_s(\mu)$ (top section), the equivalent parameter Λ_0 (middle section), and $m_r(\mu) = m(\mu)/m(M_Z)$ (bottom section) as functions of the energy scale μ. The initial values are $\alpha_s(M_Z) = 0.118$ (thick solid lines) and $\alpha_s(M_Z) = 0.115$ (thin solid lines). In the bottom section, the dots indicate the strangeness-pair-production thresholds for $m_s(M_Z) = 90\,\text{MeV}$, while crosses indicate charm-pair-production thresholds for $m_c(M_Z) = 700\,\text{MeV}$.

lines are for $\alpha_s(M_Z) = 0.115$ arising from analysis of decays of heavy quarkonium (b$\bar{\text{b}}$), and addressing an energy scale closer to our direct interest in this book.

As can be seen in the top portion of Fig. 14.1, the variation of $\alpha_s^{(2)} < 1$ (the upper index indicates the level of perturbative expansion used; see Eq. (14.21)) with the energy scale is substantial. We note the rapid change in $\alpha_s(\mu)$ at, and below, $\mu = 1$ GeV. This is not an unexpected result. However, the fact that a solution with $\alpha_s \leq 1$ governs the energy scale 1 GeV is important, since the formation of the strange quark flavor occurs in a hot QGP phase formed in experiments at 160–200A GeV (SPS–

CERN) at around 1 GeV. We can thus use the methods of perturbative QCD to study this process.

Among the parameters in Eq. (14.25), only the mass of the bottom quark plays a (hardly) noticeable role; the results shown were obtained for $m_\mathrm{s} = 0.16\,\mathrm{GeV}$, $m_\mathrm{c} = 1.5\,\mathrm{GeV}$, and $m_\mathrm{b} = 4.8\,\mathrm{GeV}$ [225]. When m_b is changed by 10%, the error on a low energy scale is barely visible. Other quark masses have less significance since the error has less opportunity to 'accumulate' in the solution of the differential equation as the energy scale decreases in the integration of Eq. (14.18).

As expected and seen in the top portion of Fig. 14.1, in the soft QGP domain $0.8\,\mathrm{GeV} < \mu < 3\,\mathrm{GeV}$, it is impossible to use a constant value of α_s. More surprisingly, the frequently used approximate inverse-logarithm form Eq. (14.12) for α_s is nearly equally inappropriate. To see this, we define a quantity $\Lambda_0(\mu)$,

$$\alpha_\mathrm{s}(\mu) \equiv \frac{2b_0^{-1}(n_\mathrm{f})}{\ln \mu^2/\Lambda_0^2(\mu)}, \quad \Lambda_0(\mu) = \mu \exp\left(-\frac{1}{b_0 \alpha_\mathrm{s}(\mu)}\right), \qquad (14.26)$$

where $\alpha_\mathrm{s}(\mu)$ is obtained in two-loop or higher-order perturbation expansion of the β-function using Eq. (14.18). The form of Eq. (14.26) is chosen to be identical to the one-loop form, compare with Eq. (14.13). Using the result for α_s shown in the top portion of Fig. 14.1, we obtain $\Lambda_0(\mu)$ seen in the middle section of the figure.

If the one-loop form Eq. (14.12) with a constant Λ_0 were a good approximation to α_s, we should see a sequence of step functions, dropping at each heavy-quark threshold. In fact, above the bottom threshold, for $\mu > 2m_\mathrm{b}$, this is nearly the case. However, below the charm threshold, for $\mu < 2.5$ GeV, where practically all QGP action is occurring, we see a rather rapid change in $\Lambda_0(\mu)$, which drops from a value near $\Lambda_0(1\,\mathrm{GeV}) \simeq 300$ MeV toward $\Lambda_0(3\,\mathrm{GeV}) \simeq 200$ MeV.

It is common to refer to the number of active quarks by using an upper index on $\Lambda_0(\mu)$, thus $\Lambda_0^{(3)}$ refers to the range $1\,\mathrm{GeV} < \mu < 2m_\mathrm{c}$, and $\Lambda_0^{(5)}$ refers to $\mu > 2m_\mathrm{b}$, and below the top threshold. We also see, in Fig. 14.1, that $\Lambda_0^{(5)} \simeq 90 \pm 15$ MeV. This value of $\Lambda_0^{(5)}$ derived from a comparison with the one-loop solution should not be mixed up with $\Lambda^{(5)} = 205 \pm 25$ MeV, which is the value required to describe α_s in the analytical two-loop solution, Eq. (14.28) [136].

To understand how quark masses depend on the energy scale, given α_s, we integrate Eq. (14.19). Substituting $m(\mu) = m_\mathrm{r}(\mu) m(M_\mathrm{Z})$, we recognize that $m_\mathrm{r}(\mu)$ is a multiplicative factor applicable to all quark masses. $m_\mathrm{r}(\mu)$ is shown in the bottom portion of Fig. 14.1. All quark masses 'run' according to this result. A quark mass given at the scale $\mu = M_\mathrm{Z}$ increases by factor 2.2 at scale $\mu = 1$ GeV, as the dotted lines drawn to

guide the eye show. Near to $\mu \simeq 1\,\text{GeV}$, the quark-mass factor $m_{\text{r}}(\mu)$ is driven by the rapid change of α_{s}. For each of the different functional dependences $\alpha_{\text{s}}(\mu)$, a different function m_{r} is found, and two results are presented, corresponding to the two cases considered in the top section of Fig. 14.1.

Since α_{s} refers to the scale of $\mu_0 = M_{\text{Z}}$, it is a convenient reference point also for quark masses. The value $m_{\text{s}}(M_{\text{Z}}) = 90 \pm 18\,\text{MeV}$ corresponds to strange-quark mass $m_{\text{s}}(1\,\text{GeV}) \simeq 195 \pm 40\,\text{MeV}$, i.e., $m_{\text{s}}(2\,\text{GeV}) \simeq 150 \pm 30\,\text{MeV}$, at the upper limit of the established range seen in table 1.1 on page 7. Similarly, we consider $m_{\text{c}}(M_{\text{Z}}) = 700 \pm 50\,\text{MeV}$, for which value we find the low-energy mass $m_{\text{c}}(1\,\text{GeV}) \simeq 1550 \pm 110\,\text{MeV}$, i.e., $m_{\text{c}}(2\,\text{GeV}) \simeq 1200 \pm 85\,\text{MeV}$, which is also at the upper limit of the accepted range, table 1.1.

For quark-pair production, the intuitive energy scale to consider is a range near to twice the (running) quark mass. Since, below $\sqrt{s} = 1$ GeV, the mass of the strange quark increases rapidly, the pair-production threshold is considerably greater than $2m_{\text{s}}(1\,\text{GeV}) \simeq 400$ MeV. The dots in the bottom portion of Fig. 14.1 show where the strangeness threshold is found, and this is at $2m_{\text{r}}(2m_{\text{s}})m_{\text{s}} = 611\,\text{MeV}$ for $\alpha_{\text{s}}(M_{\text{Z}}) = 0.118$. The strangeness threshold is where $\alpha_{\text{s}} \simeq 1$ and we can expect, considering that the phase space for pair production opens up at about $3m$, that strangeness is produced predominantly in an energy domain accessible to perturbative treatment.

For charm, the threshold shift due to running mass occurs in the opposite direction: since the mass of charmed quarks for $\mu = 1\,\text{GeV}$ is above $1\,\text{GeV}$, the production-threshold mass is smaller than $2m_c(1\,\text{GeV}) \simeq 3.1$ GeV; the production threshold is found at $\sim 2m_{\text{c}}^{\text{th}} \simeq 2.3$ GeV, and the corresponding values of m_{r} are indicated by crosses in the bottom portion of Fig. 14.1. In other words, we expect that, near the threshold, there is a slight enhancement in production of charm related to a reduction of the threshold, while the coupling strength is at $\alpha_{\text{s}}(2m_{\text{c}}) \simeq 0.3$.

The inclusion of higher-order terms in the perturbative expansion Eq. (14.21) does not influence the behavior of α_{s}. This is shown in Fig. 14.2, in which a study of α_{s} is shown. To obtain the solid line, the full current 'scheme-dependent' knowledge about the perturbative β-function is employed. The four-loop β-function obtained in the modified minimum-subtraction scheme ($\overline{\text{MS}}$) was used [136]. On the other hand, Eq. (14.21) demonstrates that there is a considerable sensitivity to the initial value $\alpha_{\text{s}}(M_{\text{Z}})$. If $\alpha_{\text{s}}(M_{\text{Z}})$ were to increase, the evaluation of the coupling strength in the 'low'-energy domain $\mu \lesssim 1$ GeV of interest here would become impossible, or at best unreliable, see the dotted lines in Fig. 14.2 above the solid line. In fact, we do not present many re-
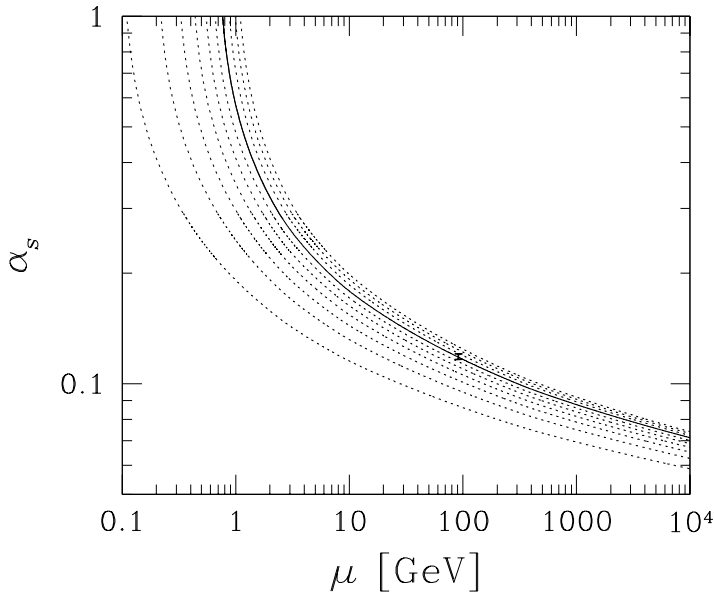
Fig. 14.2. $\alpha_s^{(4)}(\mu)$ as a function of the energy scale μ for a variety of initial conditions. Solid line, $\alpha_s(M_Z) = 0.1182$ (see the experimental point, which includes the error bar at $\mu = M_Z$); dotted lines, sensitivity to variation of the initial condition.

sults in this domain since the renormalization-group-evolution equation, Eq. (14.18), becomes numerically unstable when the four-loop perturbative β-function is used.

Interestingly, a 20% reduction in $\alpha_s(M_Z)$ leads to a 'good' $\alpha_s(0.1\,\text{GeV})$. The distance scale $1/\mu$ at which QCD becomes unstable is not just $1\,\text{fm}$, but, as this study shows, an intricate functional of the strength of the fundamental interaction, which has reliably been established only in recent years. An essential prerequirement for the perturbative theory of the production of strangeness in QGP, which we will develop in section 17.3, is the relatively small value $\alpha_s(M_Z) \simeq 0.118$.

For studying thermal processes in QGP at temperature T, the proposed interaction scale is, see Eq. (16.11),

$$\mu \equiv 2\pi T \simeq 1\,\text{GeV}\ T/T_c,$$

for $T_c \simeq 160\,\text{MeV}$. We can expect considerable sensitivity in this low range of μ to the exactness of the functional form of $\alpha_s(\mu)$, and it is necessary to use the precise function $\alpha_s(\mu)$. In Fig. 14.3, the solid line bounded by error lines corresponds to the exactly computed two-loop α_s with physical quark thresholds, Eq. (14.25), and with $\alpha_s(M_Z) = 0.1181\,\pm$
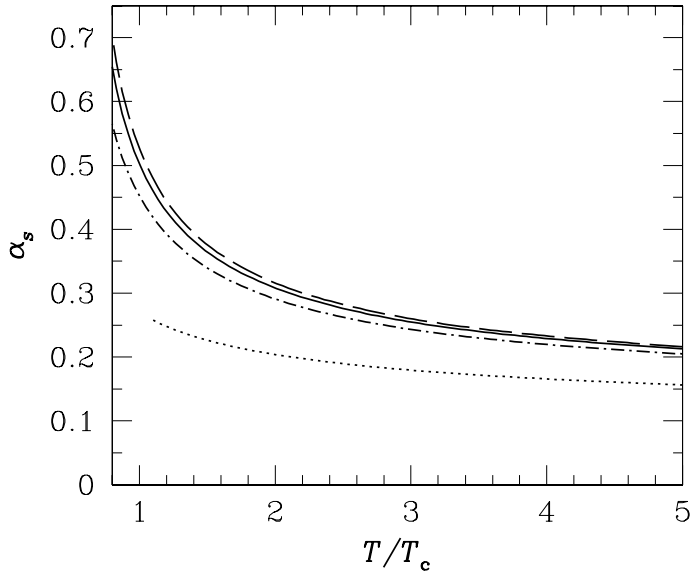
Fig. 14.3. $\alpha_s(2\pi T)$ for $T_c = 0.160\,\mathrm{GeV}$. Dashed line, $\alpha_s(M_Z) = 0.119$; solid line $= 0.1181$; chain line $= 0.1156$. Dotted line, approximate two-loop solution, given in Eq. (14.28), with the choice $\Lambda = 150$ MeV.

0.002, evaluated for the thermal scale, and expressed in terms of T/T_c. The range of experimental uncertainty in $\alpha_s(T)$, due to uncertainty in $\alpha_s(M_Z)$, is delimited by dashed and chain lines bordering the solid line in Fig. 14.3. A good approximation is obtained fitting $\alpha_s(T)$ with a logarithmic form,

$$\boxed{\alpha_s(T) \simeq \frac{\alpha_s(T_c)}{1 + C\ln(T/T_c)}, \ \ C = 0.760 \pm 0.002, \ \mathrm{for}\ T < 5T_c.} \quad (14.27)$$

The value $\alpha_s(T_c) = 0.50^{-0.05}_{+0.03}$ applies in the two-loop description with $\mu = 2\pi T$ and $T_c = 0.16$ GeV (see Fig. 14.3).

A popular approximation of α_s, which incorporates the next term beyond the one-loop logarithmic term Eq. (14.26), is

$$\overline{\alpha}_s^{(2)}(\mu) \simeq \frac{2}{b_0 \bar{L}}\left(1 - \frac{2b_1}{b_0^2}\frac{\ln \bar{L}}{\bar{L}}\right), \quad \bar{L} \equiv \ln(\mu^2/\Lambda^2). \quad (14.28)$$

$\overline{\alpha}_s^{(2)}$ agrees, using the standard value $\Lambda^{(5)} = 205 \pm 25$ MeV, with the exact solution shown at the top of Fig. 14.1, but only for $\mu > 2m_b$. On the other hand, when one is studying thermal properties of a QGP at a low energy scale the use of Eq. (14.28) below $\mu = 2m_b$ introduces considerable error, as can be seen in Fig. 14.3. Equation (14.28) is represented

by the dotted line, and misses the exact result by a factor of two, for $T_c < T < 1.75T_c$, the effective range of observables emerging from SPS and RHIC experiments. The experimental error in determination of α_s is today considerably smaller. This large difference between exact and approximate result arises, in part, because the value of $\Lambda^{(5)}$ used to obtain the thermal behavior was adjusted to be $\Lambda^{(4)} = 0.95T_c \simeq 0.15$ GeV. This value would be correct if T_c were indeed around 210 MeV, as has been thought for some time.

The high sensitivity of physical observables to α_s, makes it imperative that we do not rely on this approximation. Yet a fixed value $\alpha_s = 0.25$ (instead of $\alpha_s = 0.5$) derived from this approximation is still often used in studies of the phase properties of QGP, loss of energy by jets of partons, thermalization of charmed quarks, thermal production of strange quarks, etc. Such a treatment of thermal QCD interaction underestimates by as much as a factor of four the interaction with the QGP phase, and thus the speed of these processes. In most cases, this mundane factor matters, and we see that an accurate evaluation of α_s at the appropriate physical scale is required in order to establish the correct magnitude of these results.

15 Lattice quantum chromodynamics

15.1 The numerical approach

The perturbative approach to QCD lacks the capability to describe the long-distance behavior, which is essential for understanding the QGP–HG transformation. We need a more rigorous approach in order to characterize the physical mechanisms at the origin of color confinement, and the transition to the deconfined state of hadronic matter. A suitable nonperturbative approach is the numerical study of QCD on a lattice (L-QCD).

L-QCD is a vast field that is evolving very actively. We will limit our presentation to a pedestrian guide to the language used in this field, along with a report on a few key results of greatest importance to us. We will not be embarking on a thorough introduction to the theoretical and numerical methods. For a survey of the historical developments until the early eighties we refer to the monograph by Creutz [97], and for a summary of recent theoretical advances, and many numerical results addressing hot QCD, we refer the reader to the recent survey by Karsch [159].

The particular usefulness of the lattice-gauge-theory formulation is that it allows one to numerically carry out Feynman path integrals which represent expectation values of quantum-field-theory operators. Specifically, the expectation value of an operator $\mathcal{O}$, including both glue and quark